Fatigue State Characterization of Steel Pipes Using Ultrasonic Shear Waves

Georgios Sarris, Stewart G. Haslinger, Peter Huthwaite, and Michael J. S. Lowe

***Abstract*—The phenomenon of the reduction in the propagation speed of an ultrasonic wave when it travels through a fatigue zone has been well-studied in the literature. In addition, it has been established that shear waves are more severely affected by the presence of such a zone, compared with longitudinal waves. Our study uses these phenomena to develop a method able to characterize the fatigue state of steel pipes. Initially, the existing theory regarding the increased sensitivity of shear waves to the presence of fatigue is validated through measuring and comparing the change in propagation speed of both longitudinal and shear bulk waves on flat geometries, at different fatigue states. The comparison is achieved with the aid of ultrasonic speed C-scans of both longitudinal and shear waves, with the latter now being obtainable through our implementation of advances in electromagnetic acoustic transducers (EMATs) technology. EMATs have not been traditionally used for producing C-scans, and their ability do to so with adequate repeatability is demonstrated here; we show that shear wave scanning with EMATs now provides a possibility for inspection of fatigue damage on the inner surface of pressure-containing components in the nuclear power industry. We find that the change in ultrasonic wave speed is amplified when shear waves are used, with the magnitude of this amplification agreeing well with the theory. Following the verification of the theory, the use of EMATs allowed us to tailor the shear wave scanning method to pipe geometries, where C-scans with conventional piezoelectric transducers would not have been possible, with the results successfully revealing the presence of fatigue zones.**

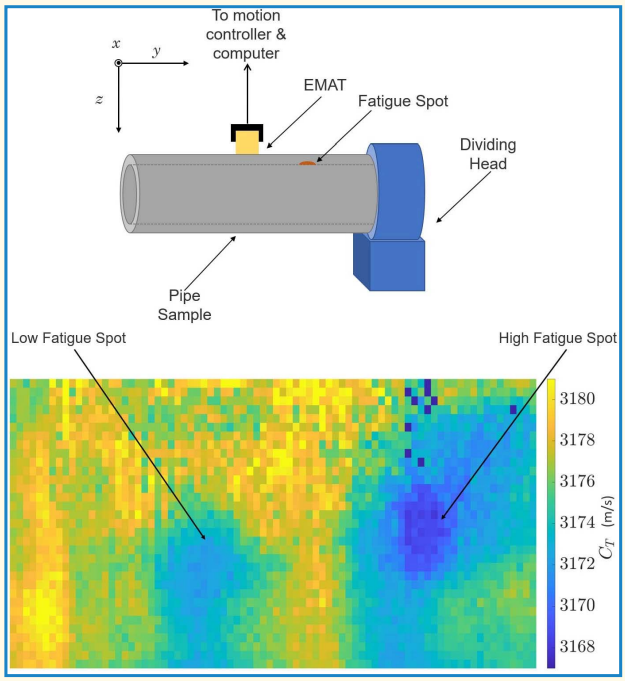

***Index Terms*—Dislocation density, electromagnetic acoustic transducers (EMATs), fatigue state, nondestructive evaluation, ultrasonic shear waves.**

I. Introduction

PRESSURE-CONTAINING components in engineering applications, such as pipes in nuclear power generation plants, which are subjected to cyclic loading, are susceptible to fatigue damage. Accurate assessment of the fatigue state of such pipes is important not only because failure can occur at stresses below the design limit of the pipe, which poses safety concerns, but also for their cost-effective monitoring and replacement.

In the literature, there is a plethora of theoretical methods which can predict the remaining life of engineering components. Examples of early life prediction theories include Paris' law and its extensions [1], [2], [3], the Palgrem–Miner rule [4], Basquin's relationship [5], and the Coffin–Manson relationship [6]. More recent advancements have allowed for more sophisticated fatigue life assessment methods, achievable through the use of Monte Carlo simulations [7], [8], probability theory and statistics [9], and fuzzy set methods [10]. However most theoretical models suffer from issues which

Manuscript received 28 September 2022; accepted 29 November 2022. Date of publication 5 December 2022; date of current version 12 January 2023. The work of Georgios Sarris was supported by the U.K. Research Centre in Nondestructive Evaluation (RCNDE) with contributions from Rolls-Royce Holdings plc and Jacobs Engineering Group Inc., under iCASE 17000191. *(Corresponding author: Georgios Sarris.)*

Georgios Sarris, Peter Huthwaite, and Michael J. S. Lowe are with Imperial College London, SW7 1AY London, U.K. (e-mail: g.sarris18@imperial.ac.uk; p.huthwaite@imperial.ac.uk; m.lowe@imperial.ac.uk).

Stewart G. Haslinger is with the Department of Mathematical Sciences, University of Liverpool, L69 7ZL Liverpool, U.K., and also with the Department of Mechanical Engineering, Imperial College London, SW7 1AY London, U.K. (e-mail: Stewart.Haslinger@liverpool.ac.uk).

Digital Object Identifier 10.1109/TUFFC.2022.3226502

Highlights

- **We demonstrated that measurements of through-thickness shear wave speed can be used to detect fatigue damage in flat plates or cylindrical pipes, where the fatigue is localized near the remote surface.**
- **It was demonstrated that shear waves are more than two times as sensitive to fatigue damage, compared with longitudinal waves.**
- **We showed that shear wave speed C-scans using EMATs with no contact or coupling medium can be obtained with the same precision as conventional longitudinal wave speed measurements.**

make them difficult or unrealistic to use in an industrial application—this is because the models require a priori knowledge of either material/component-specific constants or the cycling stress history to be used. More details about these theories and their limitations can be found in [11].

The use of ultrasound has proven to be a useful complement to fatigue state predictions in past studies, as it has been shown that ultrasonic waves are sensitive to the presence of fatigue damage, with this sensitivity manifesting as changes in their propagation speed and attenuation coefficient. This phenomenon was first explained in depth by the Granato–Lücke model [12] in which the changes in speed and attenuation coefficient of a wave when it travels through an area with an altered dislocation state are attributed to the inertia of the dislocations and the energy required to initiate and sustain their oscillation. Fatigue is a phenomenon which inherently causes changes in the dislocation state of materials [13], [14], [15], and therefore, it is possible to correlate the evolution of ultrasonic speed and/or attenuation coefficient versus the fatigue state of a component. Indeed, this has been achieved in the past—examples include axial shear wave measurements in cylindrical specimens [16], [17], [18], [19] and through-thickness shear wave measurements in [20] and [21].

Amplifying the sensitivity of a measurement to the changes in speed/attenuation is always desirable, since larger changes provide more confidence in the prediction of the fatigue state; this is because any experimental/processing errors or equipment limitations become less relevant compared with the magnitude of the change. As fatigue is usually a surface or near-surface phenomenon, one can increase the observed changes in speed by implementing measurements using surface waves, similar to [11]. Such a measurement typically necessitates direct access to the fatigued surface, which is rarely practical for in-service pipes, where fatigue damage is expected to be concentrated close to the inaccessible inner surface. The through-thickness longitudinal waves are easier to implement for local pointwise measurements; however, the changes in speed are expected to be small because the waves spend very little time in the fatigue zone.

In our study, we are proposing the use of an alternative method to amplify the changes in speed using through-thickness shear wave speed C-scans generated by electromagnetic acoustic transducers (EMATs). The possibility of using shear waves for the generation of speed C-scans provides us with two opportunities for improving the sensitivity of fatigue state measurements.

1) Shear waves are inherently more sensitive to the presence of a fatigue zone. Extensions to the Granato–Lücke model by Maurel et al. [22], [23], and [24] have shown that longitudinal and shear waves indeed behave differently to the presence of an altered dislocation state area, with the latter being inherently better at causing dislocations to vibrate—hence being more sensitive to the presence of a fatigue zone. Namely, percentage change in shear wave speed is expected to be $3\gamma^2/4$ larger than the percentage change in the longitudinal wave speed, where γ is the ratio of the longitudinal to shear wave speeds. This implies that the change in speed for shear waves will be more than double that of longitudinal waves.
2) EMATs with high fidelity and repeatability for shear waves have recently become available, allowing significantly improved sensitivity and the possibility of high-quality area scanning; this allows a more sensitive observation of deviations from the background signal than may be achieved in single-shot measurements as the presence of a zone with altered properties becomes visually obvious.

Here, we used a bespoke three-axis stepper motor frame in combination with EMATs and verified the above-mentioned increase in sensitivity, in flat geometries through the use of shear wave speed C-scans. Following this verification, we developed a method to perform shear wave speed C-scans on a pipe geometry. We also present results showing that the shear wave C-scanning method is as accurate as the more conventional longitudinal wave C-scans in terms of repeatability, and that the associated errors are significantly smaller than the expected change in speed values.

This article is organized as follows: Section II presents the theory relevant to our study, by discussing the Granato–Lücke model and its more recent extensions. Section III described the methods which we used to create the shear wave speed C-scans, both for flat and cylindrical components, while Section IV presents both the results verifying the theory in [24] in terms of wave speed changes and the extension of our scanning method to pipe geometries. Finally, Section V concludes the work.

II. Theory

This section briefly discusses the theory related to the phenomenon of ultrasonic speed reduction when a wave travels through an area with an altered dislocation state, using the Granato–Lücke model [12] and also presents the more recent findings which explain the difference in this ultrasound–dislocation interaction when longitudinal or shear waves are used.

In the Granato–Lücke model, dislocations are modeled as strings with finite length, mass, and damping. Let x and y be the horizontal and vertical components in a 2-D Cartesian coordinate system. The behavior of the dislocations under the presence of a stress wave in an elastic material is modeled using the following system of integro-differential equations:

$$\frac{\partial^2\sigma}{\partial x^2} = \rho\left(\frac{1}{G}\frac{\partial^2\sigma}{\partial t^2} + \frac{\Lambda b}{l}\frac{\partial^2}{\partial t^2}\int_0^l \xi\, dy\right) \tag{1}$$

$$A\frac{\partial^2\xi}{\partial t^2} + B\frac{\partial\xi}{\partial t} - C\frac{\partial^2\xi}{\partial y^2} = b\sigma, \quad \xi(x,0,t) = \xi(x,l,t) = 0. \tag{2}$$

Equation (1) is the linear elastic equation for a solid, with the addition of a strain term arising from the presence of the dislocations—this is the second term in the RHS of (1). Also, $\sigma(x, y, t)$ is the applied stress, t is the time, ρ is the density of the material, G is the shear modulus, Λ is the dislocation density, and b is the Burger's vector of the material. Finally, ξ is the amount by which a dislocation with length l has bowed outward due to the presence of the stress wave, like a guitar string when displaced laterally. Equation (2) describes the motion of a dislocation under an applied stress—A is the dislocation's mass, B is the damping term, and C is the tension, all normalized by the length of the dislocation. The solution of this system of equations for σ and ξ yields expressions which require the wave to indeed attenuate and reduce its propagation speed. For frequencies below the GHz range, the expressions reduce to give the following formula for the attenuation coefficient α [12], [24]:

$$\alpha = A_1 \Lambda L^4 f^2 \tag{3}$$

and relative, normalised reduction in speed, ΔC

$$\Delta C = \frac{C_f - C_h}{C_h} = -A_2 \Lambda L^2 \tag{4}$$

where L is the dislocation length, f is the frequency, and C_h and C_f are the ultrasound speed at the reference dislocation state and at the altered (hence, in our study, fatigued) dislocation state, respectively. A_1 and A_2 are constants.

Maurel et al. [24] discuss how the model in [12] encapsulates some important elements of the physics behind the dislocation–ultrasound interaction phenomenon; however, the model in [12] does not account for forests of randomly aligned dislocations or for waves with random polarizations. Using the multiple scattering theory and a small perturbation approach, Maurel et al. [24] derive expressions for the attenuation and change in speed caused by such forests of dislocations and give explicit relationships linking the dislocation state and changes in speed/attenuation for the cases where a longitudinal or shear wave travels through them. Similarly to [11], we focus this work on the speed aspect of this phenomenon.

The relative, normalised reduction in speed for a wave with w polarisation, ΔC_w, for a given dislocation state is given by [24]

$$\Delta C_w = \frac{C_{w_f} - C_{w_h}}{C_{w_h}} = Z_w \frac{\mu b^2}{\Gamma} \Lambda L^2 \tag{5}$$

where C_{w_h} and C_{w_f} are the ultrasonic speeds of a wave of w polarisation at the reference and altered dislocation states respectively, Z_w is a constant depending on whether the incident wave is shear or longitudinal, μ is the second Lamé parameter, $w = L$ for longitudinal and $w = T$ for shear waves, and Γ is a constant for a given material and dislocation state. Equation (5) is potentially difficult to quantify in a realistic inspection, due to the difficulty in measuring L and Λ for the entire volume of a real component. However, an important observation is that the ratio between the change in shear and the change in longitudinal wave speed is a constant. Given that $Z_T = (4/5\pi^4)$ and $Z_L = (16/15\pi^4\gamma^2)$ [23]

$$\frac{\Delta C_T}{\Delta C_L} = \frac{3\gamma^2}{4}. \tag{6}$$

Equation (6) implies that for steel, the changes in shear wave speed are expected to be approximately 2.5 times larger than those exhibited by longitudinal waves, for the same fatigue state, and that hence the use of shear waves is potentially beneficial in fatigue state assessment measurements.

III. Experimental Methods

Here, we present the experimental methods used to obtain wave speed C-scan maps using shear waves, as well as the benefits of those over longitudinal wave speed C-scans for the purposes of fatigue state estimations. For longitudinal waves, the methods and results were previously reported in [11], and therefore, we only present a brief summary here.

For all the measurements, a set of five fatigued plates, made by Trueflaw (Espoo, Finland), were used. The 100 × 100 × 8 mm austenitic stainless steel plates were thermally fatigued under controlled conditions using an established methodology, and each was fatigued to a different fatigue state, before the onset of cracking. For generating fatigue damage, each plate was heated to 302 °C from room temperature, in 3 s, and was then rapidly cooled and held in room temperature for another 3 s. The heat was applied locally, to a circular region with a diameter of approximately 50 mm. Details about the plates can be found in [11], but for convenience, Table I shows the number of cycles each plate had been subjected to, as well as the corresponding usage factor (UF), defined as the number of fatigue cycles over number of cycles required for failure. Trueflaw has quoted the latter to be equal to 100 000 for this set of plates. As a control, in our experiments we used a reference, blank plate, containing no fatigue damage (i.e., UF = 0).

We have also performed shear wave measurements on a steel pipe specimen. The pipe specimen had an inner diameter of 100 mm and a wall thickness of 7 mm. It contained one fatigue spot with UF = 0.24 and one with UF = 0.80.

TABLE I
TRUEFLAW PLATE'S SERIAL NUMBERS, NUMBER OF FATIGUE CYCLES (N), AND UF

Plate	00	84	91	04	99	93
N	0	17200	34400	51600	68800	86000
UF	0	0.172	0.344	0.516	0.688	0.860

A. Longitudinal Wave C-Scans

To obtain the longitudinal wave C-scans, a standard immersion tank setup was used deploying a flat-faced transducer with a center frequency of 10 MHz and an active element size equal to 0.5 in. The scanning step size was set to 0.25 mm ($\approx$ 0.43 longitudinal wavelengths), and at each point, the signal was obtained from an average of 16 measurements. The array of signals was subsequently processed into an array of C_L values.

For the C_L calculations at each point, let $s(t)$ be the recorded signal containing the first and second back wall reflections. Equation (7) gives the autocorrelated signal, $s^*(\tau)$

$$s^*(\tau) = \int_{-\infty}^{\infty} \overline{s(t)} s(t+\tau)\, dt \tag{7}$$

where $\overline{s(t)}$ is the complex conjugate of $s(t)$, and τ is a delay constant. The peaks of this autocorrelated signal were used to determine the speed by assuming a constant plate thickness of 8 mm and dividing by the time difference between those peaks. Autocorrelation was used instead of a simple time-domain analysis as it provides better signal-to-noise ratios and is less prone to errors arising from dispersion or signal distortion [25], [26].

B. Plate Shear Wave C-Scans

For the shear wave C-scans, we mounted an EMAT on a three-axis stepper motor frame, with a minimum stepping size of 2 μm. As EMATs generate ultrasound through a combination of the Lorentz, magnetic, and magnetostrictive forces [27], there is no need to couple them mechanically with the surface. This renders them more attractive than piezoelectric transducers for the generation of shear wave C-scans, as the high-viscosity couplant which they require would prohibit the stepping motion, which is necessary for the generation of C-scans, and also adversely affects the signal quality and repeatability.

The EMAT was held by a bespoke holder, and the frame allowed us to control x, y, and z coordinates of the EMAT, as shown in Fig. 1. For our investigation, we used a 2-MHz EMAT, with a circular PCB coil with a diameter of 18 mm, which was made by the non-destructive evaluation (NDE) group at Imperial College London, London, U.K., [28], [29]. The scanning step size was set to 1 mm ($\approx$ 0.75 shear wavelengths). This choice of the EMAT frequency will not disallow comparison with the longitudinal wave results, which were obtained at 10 MHz, as the theory [see (4)] suggests that changes in speed are independent of the frequency; the polarization of the EMAT is also expected to not have an effect on the detection of thermal fatigue, as it is isotropic. This frame setup is analogous to a standard, longitudinal wave

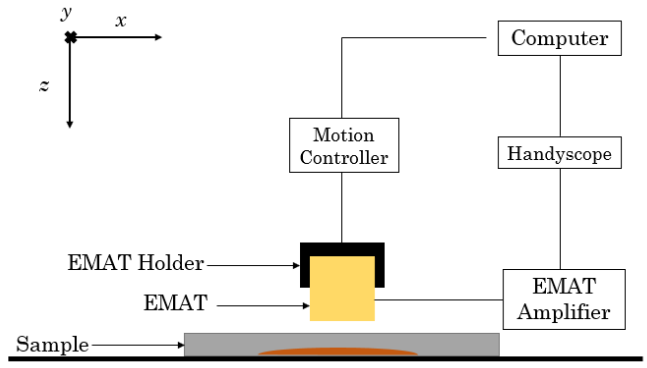

Fig. 1. Schematic of the shear wave measurements' experimental setup. The setup comprises a three-axis stepper motor frame, where the steel samples were placed, an EMAT with its excitation setup, and a transducer position controller. The orange area denotes the presence of the fatigue spot.

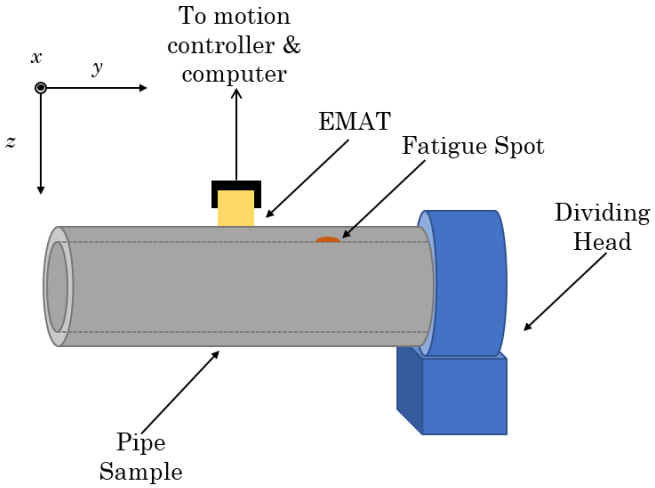

Fig. 2. Schematic of the shear wave measurements experimental setup for pipe geometries. In this setup, the EMAT is moved in the y-direction by the stepper motor frame, while rotation is achieved with the aid of the dividing head. The dashed lines denote the inner surface of the pipe sample.

C-scanning setup, with the sole difference being that our frame moves the EMAT to the desired position and stops until the required number of signals is obtained, before moving to the next point, contrary to the continuous movement of a standard immersion tank setup. For calculating the speed at each of those measurement points and generating the C_T C-scans, the same autocorrelation method described for longitudinal waves was used.

C. Shear Wave C-Scans for Pipes

The method described above was used to obtain C_T scans to compare with the C_L scans, to investigate the performance of this approach, and to verify the related theory, before moving to pipe geometries. For the pipe investigations, we used a purposely fatigued sample from Truflaw, containing two fatigue regions on the inner surface. For scanning, we used a semi-automated approach. First, the pipe sample was mounted on a dividing head. The EMAT was placed at a location offset axially from the fatigue spot, on a pristine location on the

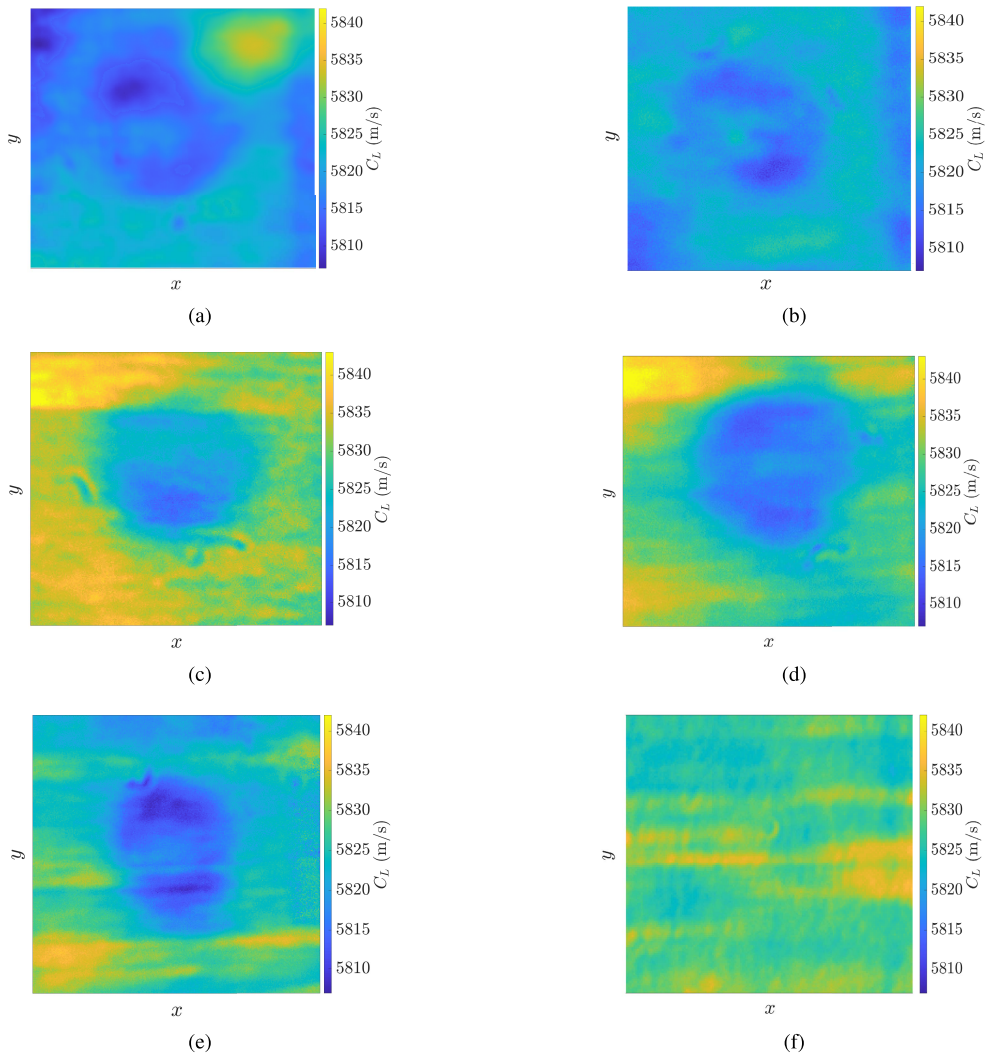

Fig. 3. C_L C-scans for the fatigued and (f) reference plates, reproduced from our work reported in [11]. The measurements were obtained by 0° through-thickness immersion testing. The results are presented in decreasing fatigue order, with parts (a)–(e) showing Plates 93, 99, 04, 91, and 84, respectively. Each plate is approximately 100 × 100 mm in size, and the fatigue spot has a diameter of approximately 50 mm.

pipe, and the scanning frame was used to move it in 1-mm increments along the major axis of the pipe (y-direction). A schematic of this setup is shown in Fig. 2. When the edge of the pipe was reached, the dividing head was manually turned by 1°, and the frame moved the EMAT back to the initial position, which was followed by another 1° turn of the dividing head. This process was repeated until the desired area was scanned, allowing for the creation of the relevant C_T scan.

IV. Results and Discussion

We present the C_L C-scan results here in summary from [11] to provide a reference for comparison to the C_T results of this present work. Fig. 3 shows the C_L maps for the five fatigued plates and a reference, blank plate. The presence of a low-speed area, corresponding to the location and size of the fatigue spot, is evident in all but the reference plate.

Using the C-scans in Fig. 3, a plot showing the variation in ΔC_L against UF was created [11], where ΔC_L is defined as

$$\Delta C_L = \frac{C_{L_f} - C_{L_h}}{C_{L_h}} \tag{8}$$

where C_{L_f} and C_{L_h} are the fatigued and healthy longitudinal wave speeds respectively. This is shown in Fig. 6. For each plate, C_{L_h} was found as the mean C_L value in an area away from the fatigue spot, and with no visible variation due to material inhomogenity, while C_{L_f} was taken as the minimum value of C_L inside the boundaries of the fatigue spot. This process is necessary as material inhomogenity creates areas of irregularities in the ultrasonic wave speed, which do not allow for simple, visual ranking of the plates in fatigue order. It was found that the change in speed decreases monotonically as fatigue progresses. The physical reason behind this observation is explained in [11]—namely, the dislocation density increases as fatigue progresses, while the dislocation loop length can be thought to be approximately constant, and therefore, using (5), the speed is indeed expected to reduce monotonically with UF. Here, it is worth noting that the minimum speed may not reduce monotonically with fatigue when comparing the five plates, but the change in speed does; this is because each change in speed value, from each plate, was calculated with respect to the speed of the material surrounding the fatigue spot, and not with respect to a constant value.

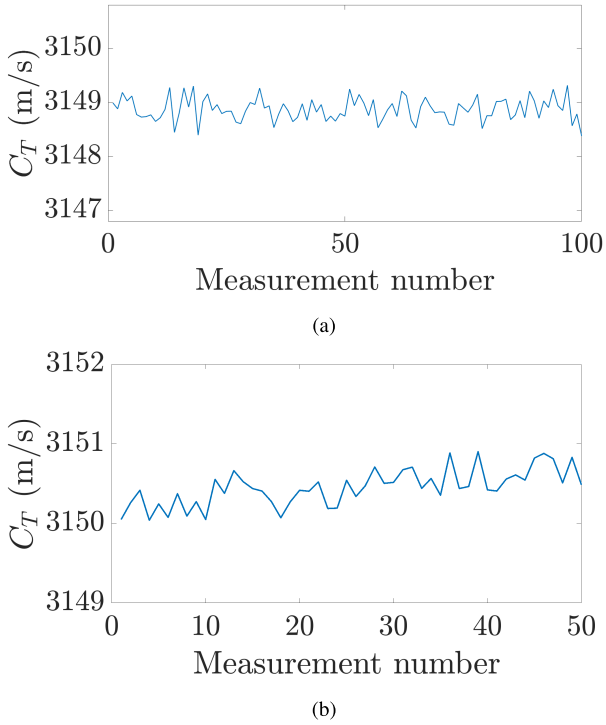

Fig. 4. Variation in C_T for the investigation of the EMAT's precision and repeatability. (a) Variation in C_T on a fixed arbitrary point on Plate 00. (b) Variation in C_T on a fixed arbitrary point on Plate 00, where the EMAT was manually lifted and placed again on the same point between measurements.

Before completing the C_T scan, we attempted to establish that the accuracy and repeatability of the EMAT were sufficient for our purposes. To measure the precision of the EMAT and the effects of electronic noise in it, we placed it on an arbitrary point on the reference plate and allowed it to complete 100 C_T measurements without moving or lifting it between measurements. To measure the repeatability of the measurements, associated with placement/alignment errors, the EMAT was placed on another arbitrary point on the healthy plate where 50 C_T measurements were taken, with the EMAT being lifted and replaced by hand between each measurement. Fig. 4 shows the results of these measurements. From the data shown in Fig. 4(a), it appears that the EMAT is performing well in terms of precision—the mean C_T value is 3148.9 m/s, and the maximum variation from this mean value is 0.012%. In addition, as shown in Fig. 4(b), the variation in speed due to placement errors is still small—the maximum absolute deviation from the mean C_T value of 3150.3 m/s is 0.014%. Both the variations are an order of magnitude smaller than the expected variation in speed due to fatigue, therefore rendering the EMAT suitable for such measurements, at least in this present context which we believe to be appropriate for inspections in the nuclear power generation industry. These results are an indication that shear waves generated by EMATs are of similar quality to those obtained from the more established immersion testing, which gives the best performance for longitudinal wave measurements.

The C_T scans of the flat samples are shown in Fig. 5. Again a clear, approximately circular area of low sound speed can be seen in all the subfigures apart from the one containing the C_T data for the reference plate. The same speed features can be seen when comparing a plate's C_L and C_T scans; for example, by comparing Fig. 3(a) with Fig. 5(a), one can observe a high speed area at the top right of both the figures. The lowest speed area can be seen in the top left quadrant of the circular fatigue spot, while overall the healthy area appears to have a larger speed value in the bottom half of the plate compared with the top half. Comparing Fig. 3(c) with Fig. 5(c), the fatigue spot appears to be slightly elongated along the horizontal axis, while there appear to be high speed bands bordering it on its left side. Analogous correlations can be seen for all the plates. This shows that the C_T scans were able to correctly identify these features as efficiently as the more established C_L scans, in terms of identifying variation in ultrasonic speed which may arise from material inhomogeneity or variations in thickness. We note that the views between the C-scans of each plate may appear different, due to small differences between the starting position of the immersion transducer and the EMAT.

To calculate the change in shear wave speed, ΔC_T, defined as

$$\Delta C_T = \frac{C_{T_f} - C_{T_h}}{C_{T_h}} \tag{9}$$

where C_{T_f} and C_{T_h} are the fatigued and healthy shear wave speeds respectively, the same method as for ΔC_L calculations was used. A plot showing the variation in ΔC_T and a comparison with ΔC_L is shown in Fig. 6.

The variation in ΔC_T is still monotonic; however, the magnitude of the change in speed is noticeably amplified. It appears that the same patterns are present in the ΔC_T curve too—the gradients of the curve between the first and second points and between the second-to-last and last points are sharper compared with the approximately linear portion in the middle of the graph. Similar to [11], the monotonic nature of ΔC_T allows for simple fatigue state estimations, as one ΔC_T value corresponds to a single point in the life of a component.

To quantify the amplification caused by the use of shear waves, each ΔC_T value in Fig. 5 was divided by its respective ΔC_L value. We believe that it is reasonable to ignore the value of the largest UF point, because as discussed in [11], the plate corresponding to this high UF value could contain identifiable cracks, which potentially renders the theory less applicable at this fatigue stage. By doing so, the mean value of the ratio (averaged over four of the plates) increases to 2.17. By substituting values for C_{L_h} and C_{T_h} in (6), the theoretical value of this ratio for our plates was found to be 2.55, which is close to the experimental value which we have obtained.

Following this verification of the theory and the ability of the EMAT to generate sufficient quality and accuracy for creating C_T C-scans, the scanning method was extended to pipe geometries. Using the method described in Section III-B, we obtained a C_T scan of a pipe containing two fatigue spots, at different fatigue states. The resulting C-scan is shown in Fig. 7.

As shown in Fig. 7, both the fatigue spots are visible. It is also evident that the left fatigue spot corresponds to a lower UF, as denoted by the lower C_T values in its vicinity.

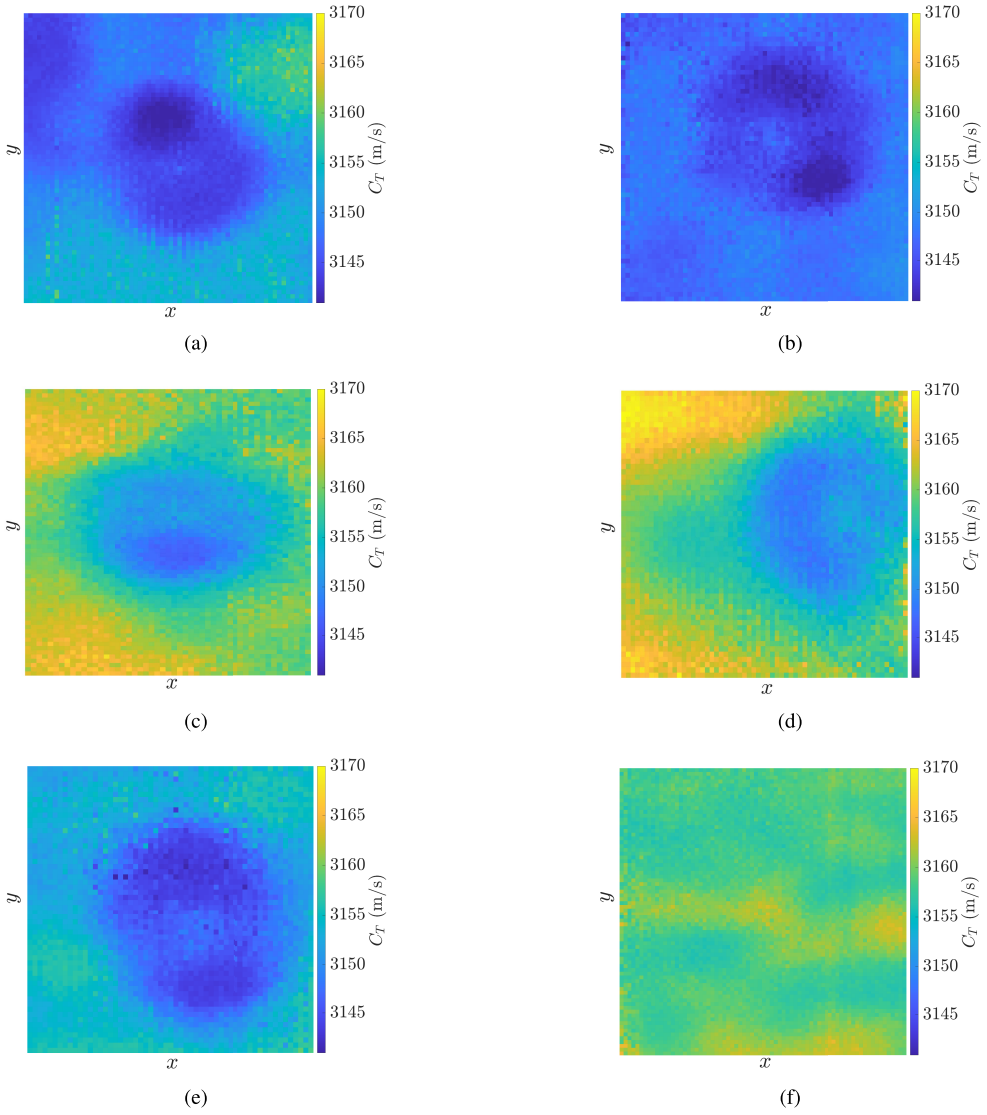

Fig. 5. C_T C-scans for the fatigued and (f) reference plates. The measurements were obtained by 0° through-thickness EMAT testing. The results are presented in decreasing fatigue order, with parts (a)–(e) showing Plates 93, 99, 04, 91, and 84, respectively. Each plate is approximately 100 × 100 mm in size, and the fatigue spot has a diameter of approximately 50 mm.

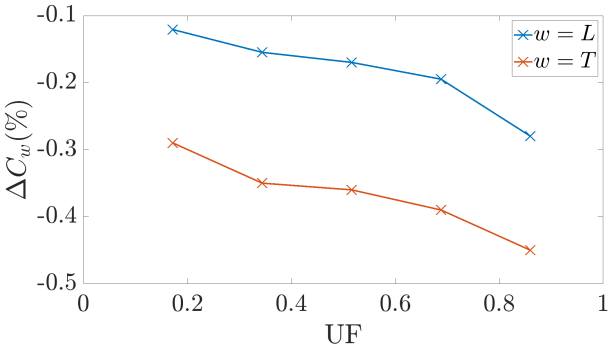

Fig. 6. Comparison of the evolution of ΔC_L and ΔC_T as the UF increases.

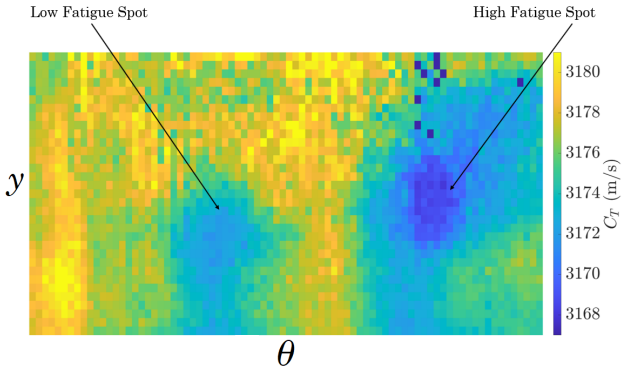

Fig. 7. C_T C-scan of the area containing the fatigue spots obtained by scanning the pipe shown schematically in Fig. 2. In this figure, y denotes the axial direction and θ denotes the circumferential direction. The size of the area scanned and presented here is approximately 150 × 100 mm.

In terms of percentage change in speed, the ΔC_T value for the left spot is −0.24%, and for the right spot it is −0.38%, calculated using the same approach of defining a healthy and a fatigued area. It also appears that the low C_T spots "leak" outside their boundaries. We believe that this indicates that heat was leaking from the heating element to the rest of the pipe during the fatiguing process. This is potentially due to the curved nature of the surface and the associated difficulty to get a complete seal between the heating element and the material. The leakage is more prominent for the high UF spot.

We propose two possible reasons. First, the higher number of cycles allows for more opportunities for heat to escape the designated fatigue spot. In addition, on the right-hand side of this fatigue spot, Trueflaw has created a third fatigue spot which further increases the possibility of heat to leak into the region between the two spots. This third spot is not shown in Fig. 7 as we were not able to record EMAT signals of adequate quality, because the sample already had identifiable cracks in that area, the presence of which has been reported by Trueflaw.

Again, it appears that an increase in fatigue cycles results in an increase in the magnitude of the ΔC_T value. According to our results in Fig. 6, the expected ΔC_T value for a UF of 0.24 and 0.80 is approximately -0.31% and -0.42%, respectively, with the latter being close to the value obtained for the respective fatigue spot in our experiment. Here, it is also worth reiterating from [11] that even though the changes in speed are monotonic, past studies have shown that even very small changes in the chemistry of the steel result in significantly different ΔC_w plots. Trueflaw does not disclose any information about the chemistry of the steel, so we cannot comment further, but we suggest that these discrepancies could be attributed to potential changes in the steel's chemistry. This also implies that each material has a unique ΔC_w versus UF curve, which needs to be used for its specific remaining life predictions.

Both in the plates and the pipe, the fatigue damage is expected to be concentrated in the near-surface of the material, meaning that bulk waves traveling through the thickness only propagate through the fatigue-damaged material for a short proportion of their journey. Nevertheless, this is enough to affect the travel time and thus to identify fatigue damage from time-of-flight measurements, even though the sensitivity is reduced by the fact that only a small zone of material is damaged.

Equation (6) is not, however, restricted to the maximum changes due to fatigue plotted in Fig. 6 and is applicable to any area with an altered dislocation state and hence can be applied to the entirety of the fatigue spot. This has the following useful implication; if a component contains an area of simply altered thickness, without any fatigue, it would appear as an area of reduced/increased speed on a C-scan, if only a single type of wave was used to complete the scan. This arises because we must assume a thickness to estimate the wave speed from distance divided by time, so any change in thickness with a single measurement is indistinguishable from a change in wave speed. However, if a C-scan is completed with both longitudinal and shear waves, it becomes possible to distinguish between the two, by converting each C-scan into a respective $\Delta C_L(\%)$ and $\Delta C_T(\%)$ map and dividing the values at each respective point. The ratio with altered dislocation state will obey (6), while in areas with altered thickness, the ratio would be equal to 1, as a thickness change affects the arrival time of any wave by the same amount.

We were able to observe this phenomenon in one of our plates. Apart from the fatigue spot, Figs. 3(b) and 5(b) show an area of reduced speed at the bottom left corner. Using the method described above, and a suitable interpolation to account for the different number of points in the two C-scans, we obtained the $\Delta C_T(\%)/\Delta C_L(\%)$ map of Plate 99, shown in Fig. 8.

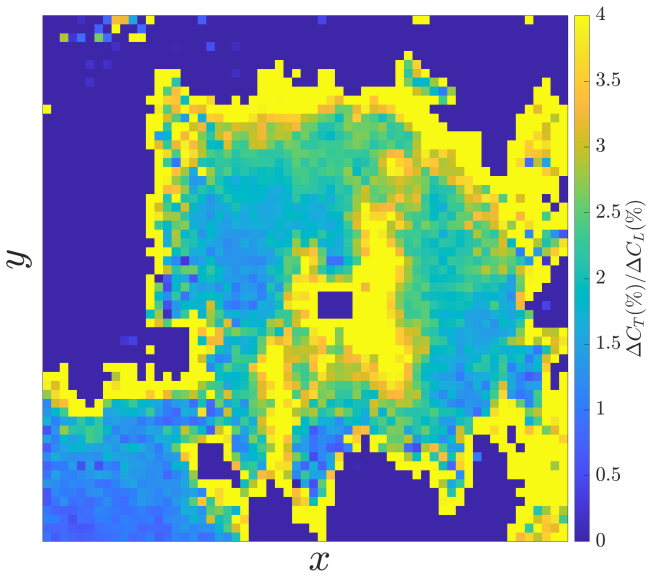

Fig. 8. $\Delta C_T(\%)/\Delta C_L(\%)$ C-scan of Plate 99, obtained by converting Figs. 3(b) and 5(b) into percentage change in speed maps, aligning them and dividing the values at each location. Here, only a detail (60 × 60 mm) of the full C-scan of this plate is shown, to emphasize the features of the fatigued area.

There are a few interesting features in Fig. 8. First, the value of the ratio inside the fatigue spot is always > 1, with most areas having a value of this ratio being approximately equal to 2–2.5. In addition, the large blue and yellow areas around the spot show that we have indeed selected correct values for C_{L_h} and C_{T_h}; this is because those areas are in the healthy region, and therefore, $\Delta C_T(\%)/\Delta C_L(\%) = 0/0$ which yields very large positive or negative values depending on the sign of the difference between the value at each of the points in the healthy area and C_{L_h} or C_{T_h}. This singularity does cause problems with the method by magnifying small discrepancies in measurements. A similar effect can be seen in the middle of the spot, where as shown in both Figs. 3(b) and 5(b), there exists a high speed area—potentially a result of uneven heating during the fatiguing process. Finally, an area where the $\Delta C_T(\%)/\Delta C_L(\%)$ value is approximately equal to 1 can be seen at the bottom left corner. We believe that this indicates the presence of an area where the plate is slightly thicker, as that area corresponds to the low-velocity regions at the bottom left corners of Figs. 3(b) and 5(b). This demonstrates the ability of our method here to distinguish between changes in speed due to thickness variations and due to fatigue, when those happen independently, although this is a preliminary observation; it would require more work to pursue this as a viable approach for inspection. It is worth highlighting that this distinction requires either a component with small thickness variation or acquisition of a time-of-flight map before the component enters service.

V. Conclusion

In this article, we developed a method for identifying the fatigue state of flat and cylindrical components, by correlating

the changes in the propagation speed of a through-thickness shear wave, with the fatigue state of a material. The assessment was completed with the aid of C_T C-scans. Although thickness measurements suffer poor sensitivity to fatigue damage because the wave spends very limited time in the fatigued region, more recent theory suggests that shear waves are inherently more sensitive to the presence of fatigue, as they are better in making the dislocations vibrate and hence exhibit a greater loss in speed when they travel inside a fatigued area [22], [23], [24].

To verify this increase in sensitivity, we used the same set of five fatigued plates as we used when we studied longitudinal wave measurements in [11]. Recent developments in EMAT technology allowed us to generate C_T C-scans for these plates, which were compared with the corresponding C_L scans in our previous study. The results showed an analogous fatigue spot to that revealed by the longitudinal wave scans, and we were also able to identify multiple common features between the C_L and C_T C-scans of each individual plate, which indicated that this scanning method yields accurate results. We subsequently calculated the percentage change in shear wave speed and the ratio between that and the percentage change in longitudinal wave speed. We found its value to be approximately 2.17, which is close to the theoretical value of 2.55, as suggested by Maurel et al. [23].

Following this verification, we completed a C_T C-scan on a pipe with two fatigue spots, with the aid of the same EMAT, and an indexing head. Our C-scan was able to reveal both the fatigue spots successfully, showing that this through-thickness shear wave measurement technique can indeed be used for fatigue state assessments in pipes, providing approximately twice the sensitivity of longitudinal waves in terms of changes in speed due to fatigue.

The results presented here provide some useful implications for future exploitation. First, it is possible to use EMATs for creating accurate C_T maps, when there is confidence in the variation in the thickness of a component. In addition, it is possible to use these scans, alongside C_L scans, to distinguish between changes in speed due to fatigue and changes in speed due to variations in thickness. Finally, C_T scanning inspections become possible on identified locations of concern, due to the high accuracy and repeatability of measurements with the EMATs, allowing measurements made at successive plant shutdowns to be compared.

Acknowledgment

The authors would like to thank Dr. Frederic Cegla and Antonio de Sanctis for their help with the experimental work in this article.

References

[1] P. Paris and F. Erdogan, "A critical analysis of crack propagation laws," *J. Basic Eng.*, vol. 85, no. 4, pp. 528–553, 1963.

[2] B. F. Spencer and J. Tang, "Markov process model for fatigue crack growth," *J. Eng. Mech.*, vol. 114, no. 12, pp. 2134–2157, Dec. 1988.

[3] J. C. Newman, "A crack-closure model for predicting fatigue crack growth under aircraft spectrum loading," *Amer. Soc. Testing Mater.*, 1981.

[4] M. A. Miner, "Cumulative damage in fatigue," *J. Appl. Mech.*, vol. 12, no. 3, pp. A159–A164, 1945.

[5] O. H. Basquin, "The exponential law of endurance tests," in *Proc. Amer. Soc. Test. Mater.*, vol. 10, 1910, pp. 625–630.

[6] L. F. Coffin, "A study of the effects of cyclic thermal stresses on a ductile metal," *J. Fluids Eng.*, vol. 76, no. 6, pp. 931–949, Aug. 1954.

[7] M. T. Todinov, "Probability distribution of fatigue life controlled by defects," *Comput. Struct.*, vol. 79, no. 3, pp. 313–318, Jan. 2001.

[8] M. T. Todinov, "A probabilistic method for predicting fatigue life controlled by defects," *Mater. Sci. Eng., A*, vol. 255, nos. 1–2, pp. 117–123, Oct. 1998.

[9] J. Y. Kim, J. H. Lee, and S. H. Nahm, "Statistical analysis of casting defects in microstructure for understanding the effect on fatigue property of 17–4PH stainless steel," *Key Eng. Mater.*, vols. 321–323, pp. 1503–1506, Oct. 2006.

[10] S.-P. Zhu, H.-Z. Huang, and Z.-L. Wang, "Fatigue life estimation considering damaging and strengthening of low amplitude loads under different load sequences using fuzzy sets approach," *Int. J. Damage Mech.*, vol. 20, no. 6, pp. 876–899, Aug. 2011.

[11] G. Sarris, S. G. Haslinger, P. Huthwaite, and M. J. S. Lowe, "Ultrasonic methods for the detection of near surface fatigue damage," *NDT&E Int.*, to be published.

[12] A. Granato and K. Lücke, "Theory of mechanical damping due to dislocations," *J. Appl. Phys.*, vol. 27, no. 6, pp. 583–593, Jun. 1956.

[13] W. A. Wood, "Formation of fatigue cracks," *Phil. Mag.*, vol. 3, no. 31, pp. 692–699, Jul. 1958.

[14] N. F. Mott, "A theory of the origin of fatigue cracks," *Acta Metallurgica*, vol. 6, no. 3, pp. 195–197, Mar. 1958.

[15] F. C. Frank and W. T. Read, "Multiplication processes for slow moving dislocations," *Phys. Rev.*, vol. 79, no. 4, pp. 722–723, 1950.

[16] T. Ohtani, K. Nishiyama, S. Yoshikawa, H. Ogi, and M. Hirao, "Ultrasonic attenuation and microstructural evolution throughout tension–compression fatigue of a low-carbon steel," *Mater. Sci. Eng., A*, vol. 442, nos. 1–2, pp. 466–470, Dec. 2006.

[17] T. Ohtani, H. Ogi, Y. Minami, and M. Hirao, "Ultrasonic attenuation monitoring of fatigue damage in low carbon steels with electromagnetic acoustic resonance (EMAR)," *J. Alloys Compounds*, vol. 310, nos. 1–2, pp. 440–444, Sep. 2000.

[18] H. Ogi, T. Hamaguchi, and M. Hirao, "In-situ monitoring of ultrasonic attenuation during rotating bending fatigue of carbon steel with electromagnetic acoustic resonance," *J. Alloys Compounds*, vol. 310, nos. 1–2, pp. 436–439, Sep. 2000.

[19] M. Hirao, H. Ogi, N. Suzuki, and T. Ohtani, "Ultrasonic attenuation peak during fatigue of polycrystalline copper," *Acta Mater.*, vol. 48, no. 2, pp. 517–524, Jan. 2000.

[20] A. Sorich, M. Smaga, and D. Eifler, "Fatigue monitoring of austenitic steels with electromagnetic acoustic transducers (EMATs)," *Mater. Perform. Characterization*, vol. 4, no. 2, Feb. 2015, Art. no. 20140017.

[21] S. Kenderian, T. P. Berndt, R. E. Green, and B. B. Djordjevic, "Ultrasonic monitoring of dislocations during fatigue of pearlitic rail steel," *Mater. Sci. Eng., A*, vol. 348, nos. 1–2, pp. 90–99, May 2003.

[22] A. Maurel, J.-F. Mercier, and F. Lund, "Scattering of an elastic wave by a single dislocation," *J. Acoust. Soc. Amer.*, vol. 115, no. 6, pp. 2773–2780, Jun. 2004.

[23] A. Maurel, J.-F. Mercier, and F. Lund, "Elastic wave propagation through a random array of dislocations," *Phys. Rev. B, Condens. Matter*, vol. 70, no. 2, Jul. 2004, Art. no. 024303.

[24] A. Maurel, V. Pagneux, F. Barra, and F. Lund, "Wave propagation through a random array of pinned dislocations: Velocity change and attenuation in a generalized granato and Lücke theory," *Phys. Rev. B, Condens. Matter*, vol. 72, no. 17, Nov. 2005, Art. no. 174111.

[25] J. Isla and F. Cegla, "Coded excitation for low SNR pulse-echo systems: Enabling quasi-real-time low-power EMATs," in *Proc. IEEE Int. Ultrason. Symp. (IUS)*, Sep. 2016, pp. 1–4.

[26] A. Gajdacsi and F. Cegla, "The effect of corrosion induced surface morphology changes on ultrasonically monitored corrosion rates," *Smart Mater. Struct.*, vol. 25, no. 11, Nov. 2016, Art. no. 115010.

[27] M. Hirao and H. Ogi, *EMATs for Science and Industry*. Norwell, MA, USA: Kluwer, 2003.

[28] J. Isla and F. Cegla, "Optimization of the bias magnetic field of shear wave EMATs," *IEEE Trans. Ultrason., Ferroelectr., Freq. Control*, vol. 63, no. 8, pp. 1148–1160, Aug. 2016.

[29] J. Parra-Raad, P. Khalili, and F. Cegla, "Shear waves with orthogonal polarisations for thickness measurement and crack detection using EMATs," *NDT E Int.*, vol. 111, Apr. 2020, Art. no. 102212.